Time-resolved detection of spin-spatial-coupling-induced dynamical phase transitions

J. O. Austin-Harris,* Z. N. Hardesty-Shaw, C. Binegar, P. Sigdel, N. Rago, T. Bilitewski, and Y. Liu†
Department of Physics, Oklahoma State University, Stillwater, Oklahoma 74078, USA

(Received 3 April 2026; accepted 10 August 2026; published 28 August 2026)

We demonstrate the time-resolved detection of dynamical phase transitions (DPTs) in lattice-confined spinor gases subject to *a priori* unknown time-variant interactions, via the temporal behaviors of both the system energy and spinor phases extracted from the observed spin dynamics. Using this technique, we describe the observed nonequilibrium spin dynamics, governed by intricate spin-spatial couplings, across a range of conditions. This work also introduces a diagnostic tool that can quickly identify DPTs without requiring observations over at least a full period of the spin dynamics. Our approach can naturally extend to other complex systems subject to time-dependent parameters, such as Floquet systems under driven magnetic fields, driven interactions, or spin-flopping fields, with potential applications in the study of DPTs in nonintegrable models.

DOI: 10.1103/bl8c-sdhy

I. INTRODUCTION

Ultracold spinor gases, highly controllable quantum systems with a spin degree of freedom, have been proposed as ideal platforms for studying nonequilibrium phenomena [1–15]. When out of equilibrium, spinor gases display spin oscillations driven by the competition of the quadratic Zeeman energy q and the spin-dependent interactions c_2 [1–9,16–27]. These spin oscillations reveal a rich dynamical phase diagram hosting dynamical phase transitions (DPTs) [11–15,28,29] that can be engineered through various modifications to system parameters.

DPTs are of fundamental interest due to their association with universal nonequilibrium critical phenomena and as pathways to quantum-enhanced sensing and quantum entanglement [11–15,28,29]. There are two categories of DPTs recognized in the literature: type-I DPTs, characterized by an order parameter, typically the long-time average of an observable, that varies nonanalytically with a quenched control parameter, and type-II DPTs, which display nonanalytic temporal behavior in a global order parameter after a quench [11–14]. The study of DPTs has been accomplished both experimentally and theoretically in a wide variety of systems, including condensed matter systems [13,30,31], trapped ions [12,13,28,32–34], and both scalar and spinor ultracold gases [10–15,23,29]. However, these investigations have thus far been primarily limited to systems that are well understood theoretically, such as integrable systems [13,28,34].

In this work, we demonstrate the time-resolved detection of type-I DPTs first in a simple well-understood system, i.e., spinor gases in free space, and then in a lattice-confined spinor system with *a priori* unknown time-variant interactions, via temporal behaviors of spinor phases and system energy extracted from observed spin dynamics. Realizing DPT detection in systems with unknown time-dependent system parameters opens an avenue for the study of crossover phenomena, universality, and DPTs in nonintegrable models, such as in spinor gases subject to weak spin-flopping fields, which can host quantum scars and quantum many-body scars [13,23,26,28,35]. We also introduce a diagnostic tool, the cutoff time t_c, to quickly identify DPTs without requiring observations over at least one full period of the spin dynamics. The success of our informed predictions, especially in explaining the observed spin dynamics manipulated by intricate spatial dynamics over a range of conditions, suggests that similar techniques can be applied to analyze observations in other complex systems with time-dependent parameters, e.g., Floquet systems under driven quadratic Zeeman shift q [36–39], driven interaction c_2 [5,10], or resonant spin-flopping fields [23,26,35].

II. EXPERIMENTAL SEQUENCE

Each experimental cycle begins with an $F = 1$ spinor Bose-Einstein condensate of up to 10^5 sodium atoms in a crossed optical dipole trap (ODT) of trapping frequencies $\omega_{x,y,z} \sim 2\pi \times (120, 120, 160)$ Hz. At holding time $t = 0$ we prepare an initial state with $\rho_0(0) \approx 0.45$, $M(0) = 0$, and $\theta(0) = 0$. Here $\theta = \theta_1 + \theta_{-1} - 2\theta_0$ is the relative spinor phase, and θ_{m_F} (ρ_{m_F}) is the phase (fractional population) of the m_F hyperfine spin state. We note that the magnetization $M = \rho_1 - \rho_{-1}$ is conserved when no external driving field is applied. We demonstrate the time-resolved detection of DPTs induced via one of two experimental sequences, Quench-Q and moving-lattice sequences (see Fig. 1). These sequences result in time-variant ratios q/c_2 enabling us to engineer the dynamical phase diagram. Quench-Q sequences use magnetic field quenches to induce a time-variant q as a control parameter. Moving-lattice sequences impart an *a priori* unknown time variance to c_2 using a one-dimensional (1D) moving lattice constructed from two nearly orthogonal lattice beams that are skew to both ODT beams. In these sequences [see Fig. 1(b)], the atoms are first adiabatically loaded into a shallow stationary lattice with a depth of $2E_R$, where E_R is the recoil energy.

*Contact author: jared.o.austin@okstate.edu
†Contact author: yingmei.liu@okstate.edu

 ©2026 American Physical Society

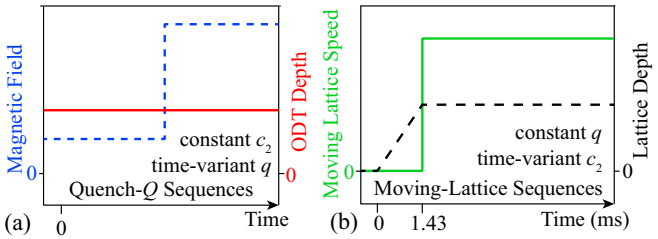

FIG. 1. (a) Schematic of Quench-Q sequences showing how the magnetic field (blue) and ODT trapping depth (red) vary in time. (b) Schematic of moving-lattice sequences showing how the lattice speed (green) and lattice depth (black) vary in time. Axes are not to scale in both panels.

The frequency difference between the lattice beams is then quenched from 0 to $\Delta f = 4.6E_R/h$, which accelerates the lattice speed to $v = \lambda_L \Delta f$. The moving lattice then near resonantly couples the $\mathbf{p} = 0$ and $\mathbf{p} = 2\hbar\mathbf{k}_L$ momentum states and induces a time-variant c_2 via the coupling of spin and spatial degrees of freedom [6,40]. Here $\lambda_L/2 \approx 810$ nm is the lattice spacing, $\mathbf{k}_L$ is the lattice wave vector, and h ($\hbar$) is the (reduced) Planck constant. At the end of an experimental cycle, atoms are released from all trapping potentials for ballistic expansion and spin-resolved imaging.

III. MODEL

For the data presented in this work, all spin states appear to share a common but potentially time-dependent spatial mode. Combined with the calculated spin healing length ($\approx$12 μm) being larger than the Thomas-Fermi radii ($\approx$(9, 9, 7) μm) for the typical initial atom numbers ($\approx 10^5$) studied in this work, this supports the use of a dynamical single spatial-mode approximation (SMA) to express the system Hamiltonian [6]:

$$H/h = c_2\rho_0[1-\rho_0+\sqrt{(1-\rho_0)^2-M^2}\cos(\theta)] + q(1-\rho_0). \quad (1)$$

With the exception that c_2 and q may be time dependent rather than strictly constant, Eq. (1) is identical to the well-known SMA-based Hamiltonian of $F = 1$ spinor gases in free space [1–6,17–25]. Although the SMA was traditionally considered valid only for frozen spatial modes, recent work demonstrates that it remains applicable if all spin states share the same time-dependent spatial mode [5,6,10]. This is the case for our moving-lattice system: the observed complex spatial dynamics are found to be nearly identical for all spin states, which also agrees with a predicted near-unity overlap in the spatial modes between spin states in this system (see Sec. V and Ref. [6]).

Equation (1) results in the following equations of motion for ρ_0 and θ [3,4,17,21,23],

$$\frac{\partial\rho_0}{\partial t} = \frac{-2}{\hbar}\frac{\partial H}{\partial\theta} = \frac{c_2}{\pi}\rho_0\sqrt{(1-\rho_0)^2-M^2}\sin(\theta), \quad (2)$$

$$\frac{\partial\theta}{\partial t} = \frac{2}{\hbar}\frac{\partial H}{\partial\rho_0} = \frac{c_2}{\pi}\frac{(1-\rho_0)(1-2\rho_0)-M^2}{\sqrt{(1-\rho_0)^2-M^2}}\cos(\theta) + \frac{c_2}{\pi}(1-2\rho_0) - \frac{q}{\pi}. \quad (3)$$

By approximating time derivatives as discrete differences evaluated based on the observed population dynamics, the equations of motion can be consistently solved for c_2 and θ to construct a complete picture of the full quantum dynamics (see Appendix A). Two distinct dynamical regimes are predicted by these equations of motion: an interaction-dominated regime where θ is bounded within $|\theta| < \pi/2$ [see red curves in Figs. 2(a) and 2(b)] and a Zeeman-dominated regime where θ is unbounded [see blue curves in Figs. 2(a) and 2(b)] [5,6].

IV. TIME-RESOLVED DETECTION OF DPTs

Our experimental data in Figs. 2(a) and 2(b) reveal DPTs induced by quenching q at approximately the minimum ($\rho_0 \approx 0.12$) and maximum ($\rho_0 \approx 0.42$) of the prequench ρ_0 oscillation, respectively. Initially, the system is in the interaction regime with bounded θ (following a closed path in the phase diagram). After the q quench, θ becomes unbounded marking a DPT to the Zeeman regime. These observations can be described by Eq. (1) with a constant $c_2 \approx 22$ Hz and $q = 15$ Hz before ($q = 41$ Hz after) the quench, as shown by the red (blue) energy contours in Figs. 2(a) and 2(b). Here θ is extracted from the observed spin population dynamics by using the time-variant system parameters [e.g., $q(t)$ in this section and $c_2(t)$ in Sec. V] in Eqs. (2) and (3). By approximating $\frac{\partial\rho_0}{\partial t}$ as the discrete difference between ρ_0 data points, Eq. (2) can first be solved for possible θ points. Then to unwrap the phase, we can minimize the difference between $\frac{\partial\theta}{\partial t}$ as calculated from Eq. (3) and the discrete difference between possible θ points. This extends the technique developed in our prior work [23] to a dynamical SMA model by including information about the time variance of system parameters into the phase extraction.

Figures 2(a) and 2(b) show that time traces of the phase θ provide a rigorous characterization of the dynamical phase diagram and DPTs, while, in contrast, evolution of spin populations ρ_{m_F} alone cannot directly identify what regime of the phase diagram the system is in without comparison to the theoretical phase diagram. We therefore focus on the temporal behavior of phase-based observables when studying DPTs in this work.

For sharper time-resolved identification of the DPTs, we plot the extracted $\cos(\theta/2)$ in Fig. 2(c) for the two experiments shown in Figs. 2(a) and 2(b), as well as a control set in which q remains constant. For the two sets where q was quenched, the experimental $\cos(\theta/2)$ begins significantly changing with time shortly after the quench, while in contrast $\cos(\theta/2)$ remains close to one for the control set [see Fig. 2(c)]. These observations are consistent with SMA predictions: in the interaction regime $\cos(\theta/2)$ has a tiny peak-to-peak amplitude, while in the Zeeman regime $\cos(\theta/2)$ oscillates between ± 1. Therefore, a significant change in $\cos(\theta/2)$ indicates a DPT from the interaction to the Zeeman regime has occurred in our experiments. To quantify this behavior, we define the cutoff time t_c as the time at which θ first satisfies $|\theta| > \pi/2$, corresponding to $\cos(\theta/2) < 0.7$, and becomes inconsistent with observations in the interaction regime [see Fig. 2(c)].

Strictly speaking, the rigorous detection of a DPT requires observing a nonanalytic change in an order parameter as a

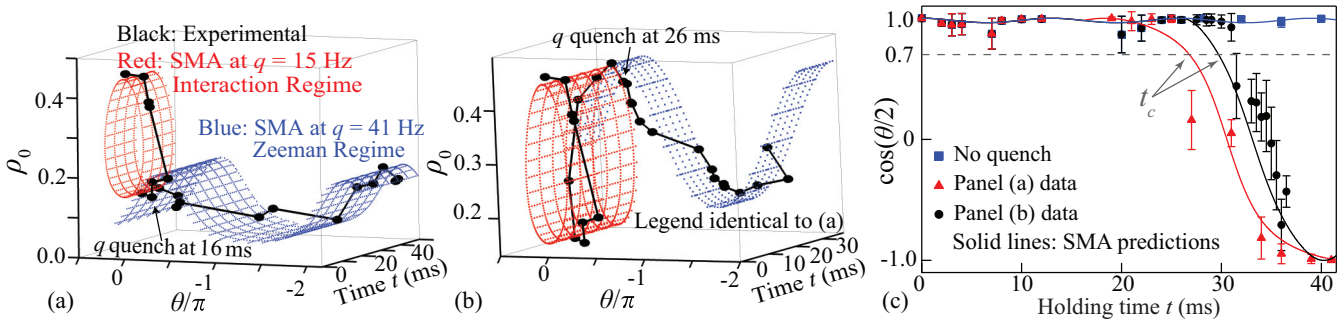

FIG. 2. (a) Black circles show a DPT from an interaction regime to a Zeeman regime observed after a Quench-Q sequence, a sudden quench in q from 15 to 41 Hz at 16 ms with the timing of the quench roughly corresponding to a minimum in the ρ_0 oscillation where $\rho_0 \approx 0.12$ and $\theta \approx 0$. Red (blue) dotted surfaces display the SMA equal energy contours of the interaction (Zeeman) regime occurring before (after) the q quench for our system where $c_2 \approx 22$ Hz and $M = 0$ [see Eq. (1)]. (b) Similar to panel (a) but taken with the quench at 26 ms roughly corresponding to a maximum in the ρ_0 oscillation where $\rho_0 \approx 0.42$ and $\theta \approx 0$. (c) Triangles (circles) show that the extracted $\cos(\theta/2)$ identifies the DPTs after the q quenches at 16 ms (26 ms), while squares indicate no DPT occurs without a q quench. Solid lines are SMA predictions, while the intersection of the dashed and solid lines marks the cutoff time t_c where the system is conclusively shown to be in the Zeeman regime (see text).

control parameter is varied. However, the similar dependence of t_c and a typical order parameter β on the control parameter q/c_2 confirms that t_c can also be used to observe the DPT [see Fig. 3(a)]. Here $\beta = 2 - A_{\rm pp}$, with $A_{\rm pp}$ being the peak-to-peak amplitude of a full period of $\cos(\theta/2)$. The time needed to meaningfully measure t_c and β, denoted T_{t_c} and T_β, respectively, depends on the state during the quench. Notably, T_{t_c} is predicted to be always shorter than or equal to T_β, as shown for a typical initial state in Fig. 3(b). Intuitively, t_c can be determined from a handful of observations after the quench. In contrast, multiple observations over at minimum a full period of the spin dynamics are required to determine

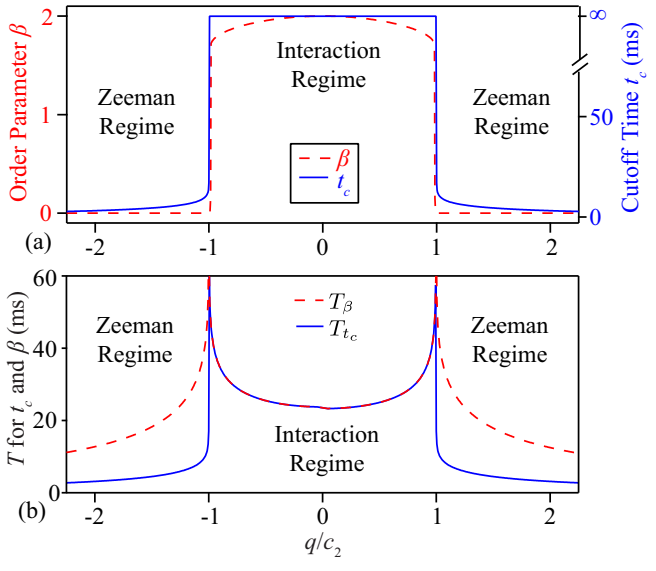

FIG. 3. (a) The similarities in the predicted dependence of the cutoff time t_c (solid line) and the order parameter β (dashed line) on q/c_2 confirm that t_c is a good observable for detecting DPTs. (b) T_{t_c} (solid line), the time needed to determine the cutoff time t_c, is always shorter than or equal to T_β (dashed line), the time needed to determine β. In both panels, predictions are based on Eq. (1) for our system using a typical initial state in which $\rho_0(0) = 0.5$ and $\theta(0) = 0$.

commonly used order parameters, e.g., β, or similar observables based on the time average or oscillation amplitude of $\cos(\theta/2)$ [10,12,23], winding number of θ [15], or the time average or steady-state behavior of ρ_0 [10,11,14,29].

V. SPIN-SPATIAL-COUPLING-INDUCED DPTs

Having established that $\cos(\theta/2)$ distinguishes distinct dynamical regimes of $F = 1$ spinor gases and t_c more sharply identifies DPTs in time for the case where the system is well understood in theory (see Fig. 2), we extend the analysis to a much more complicated moving-lattice system (see Fig. 4). This demonstrates the technique's applicability even with limited knowledge of system parameters or theory predictions. The moving-lattice sequence transfers a significant fraction of the atoms to the $\mathbf{p} = 2\hbar\mathbf{k}_L$ momentum state, and these atoms are slowed as they move away from the minima of the ODT potential. The interplay between the ODT and the moving lattice causes complex spatial dynamics and rapid number loss, modifying the atomic density and thereby the interactions governing spin dynamics [6].

These violent spatial dynamics make standard methods of obtaining the value of c_2, whether from the estimated experimental atomic density or theoretical modeling, less reliable; as the spatial dynamics are highly sensitive to a large number of system parameters [6]. Instead the observed spin dynamics can be utilized to reliably estimate c_2 through iteratively first solving Eq. (2) for θ and then Eq. (3) for c_2, provided $\rho_0(t)$ is not close to 0.5 and the system remains in the interaction regime (see Fig. 4(a) and Ref. [23]). This method requires a time point where all relevant system parameters are known, and, while the initial state and q can be precisely measured, $c_2(0)$ must be estimated. Figures 4(a) and 4(b) demonstrate that the simultaneously extracted c_2 and θ curves rapidly converge regardless of the initial estimate for $c_2(0)$, confirming that the extracted values faithfully reflect the information carried in the spin population dynamics. The robustness of the extraction enables its use even in highly nonequilibrium systems where system parameters may not be precisely known, for example, in the moving-lattice system [see Figs. 4(c)–4(e)].

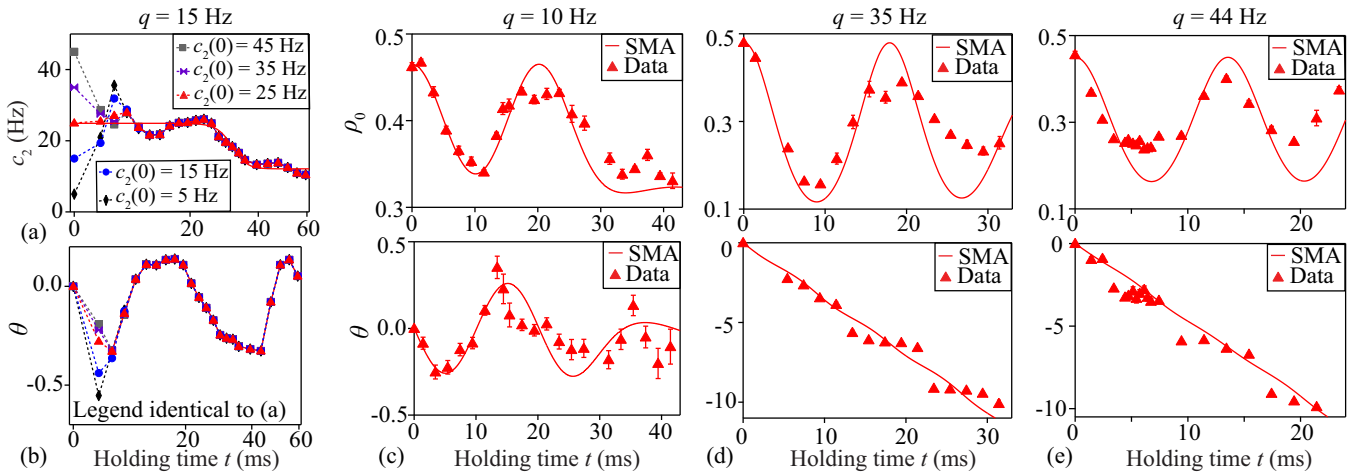

FIG. 4. Markers display (a) $c_2(t)$ and (b) $\theta(t)$, extracted from observed spin population dynamics at $q = 15$ Hz, quickly converge despite drastically different initial guesses for $c_2(0)$. The red solid line in panel (a) is a sigmoidal fitting curve to the $c_2(0) = 25$ Hz dataset. (c) Upper panel: Triangles show the observed ρ_0 time evolution at $q = 10$ Hz after the moving-lattice sequence. Lower panel: Triangles display the corresponding θ extracted from the spin population dynamics utilizing $c_2(t)$ based on the fitting shown in panel (a). Lines in both subpanels display SMA predictions [see Eq. (1)] based on the fitting shown in panel (a). (d), (e) Similar to panel (c) but at (d) $q = 35$ Hz and (e) $q = 44$ Hz.

To extend the analysis across a broad range of q in the moving-lattice system, we use an estimate of c_2, provided by the fitting curve [the solid line in Fig. 4(a)], to extract θ and predict the behavior of the system at other q. This transfer of the extracted interaction c_2 to other q is supported by the similarities in the extracted $c_2(t)$ for datasets taken at different q values and also by similarities in the spatial dynamics and the rate of atom number loss observed at all q values studied (see Appendix B). Additional support is provided by theoretical simulations which show excellent agreement between SMA predictions that utilize a time-dependent c_2 derived from scalar 1D Gross-Pitaevskii (GP) simulations (in which c_2 is explicitly independent of q and all spin states share a common time-dependent spatial mode) and full spinor 1D GP simulations (in which c_2 could potentially be q dependent and multimodal effects are allowed) [6]. These 1D simulations qualitatively describe key elements of the moving-lattice system, e.g., the spatial dynamics and spin dynamics, by accounting for all confining potentials, the effects of gravity, and atom losses associated with the finite ODT size, although a full theoretical treatment of the moving-lattice system requires computationally challenging three-dimensional simulations [6]. The excellent agreement between the two 1D simulations indicates that the fundamental assumptions of the SMA predictions, including that $c_2(t)$ is q independent, are valid. We demonstrate this extension in Fig. 4(c) [Figs. 4(d) and 4(e)], which shows a typical example at $q = 10$ Hz ($q = 35$ Hz and $q = 44$ Hz), where the system remains in the interaction (Zeeman) regime throughout the dynamics with bounded (unbounded) θ, and the dynamics are fairly well captured by the SMA predictions informed by the $c_2(t)$ fitting curve.

While datasets featured in Fig. 4 remain in a single dynamical regime throughout the dynamics, a comparison of moving-lattice datasets taken at different q values [see Fig. 5(a)] demonstrates that at an appropriate q value the system undergoes a DPT driven by the moving-lattice-induced change in c_2 from $c_2 \approx 25$ Hz at $t = 0$ to $c_2 \approx 12$ Hz at $t \gg 0$. As seen in Fig. 5(a), after a long initial plateau near 1, the observable $\cos(\theta/2)$ drops below 0.7 for the $q = 20$ Hz dataset (blue circles) at $t_c \approx 40$ ms, indicating that a DPT has occurred, while in contrast $\cos(\theta/2)$ remains close to 1 for all t in the $q = 15$ Hz dataset (red triangles), indicating no DPT occurs. The moving-lattice-tuned phase diagram and DPT at $q = 20$ Hz can also be well described by equal energy contours predicted by Eq. (1) for a constant $c_2 = 25$ Hz $\approx c_2$ ($t = 0$) before (green dotted line) and $c_2 = 12$ Hz $\approx c_2$ ($t \gg 0$) after (black dotted line) an effective c_2 quench induced by the moving lattices [see Fig. 5(a) inset].

We can confirm these observations, i.e., that the moving-lattice system undergoes (does not undergo) a DPT when $q = 20$ Hz ($q = 15$ Hz), by examining the energy E of the system. Here E can be readily evaluated from Eq. (1) once θ and c_2 are known. The separatrix that separates the Zeeman and interaction regimes in the phase diagram of $F = 1$ spinor gases lies along the energy contour where $E = E_{\text{sep}}$ and $E_{\text{sep}} = h \cdot q$ if the magnetization $M = 0$ [19]. The energy E provides a complementary view of the physics underlying the DPT, while $\cos(\theta/2)$ offers visually distinct behavior between the regimes without required knowledge of a potentially time-dependent q such as in the data presented in Fig. 2. In Fig. 5(b), both the $q = 15$ Hz (red) and $q = 20$ Hz (blue) datasets start firmly in the interaction regime where $E > E_{\text{sep}}$. As c_2 decreases due to the violent spatial dynamics and atom number loss in the moving-lattice system, E decreases correspondingly. For the $q = 20$ Hz dataset, this decrease in E results in the system crossing the separatrix and undergoing a DPT, i.e., $E < E_{\text{sep}}$ for $t \gtrsim 35$ ms; while for the $q = 15$ Hz data set, E remains larger than E_{sep} for all holding times studied and therefore the system does not undergo a DPT [see Fig. 5(b)]. Therefore the observations in Fig. 5 confirm that θ, t_c, and E can be used for the time-resolved detection of DPTs in a system with *a priori* unknown system parameters utilizing the presented techniques.

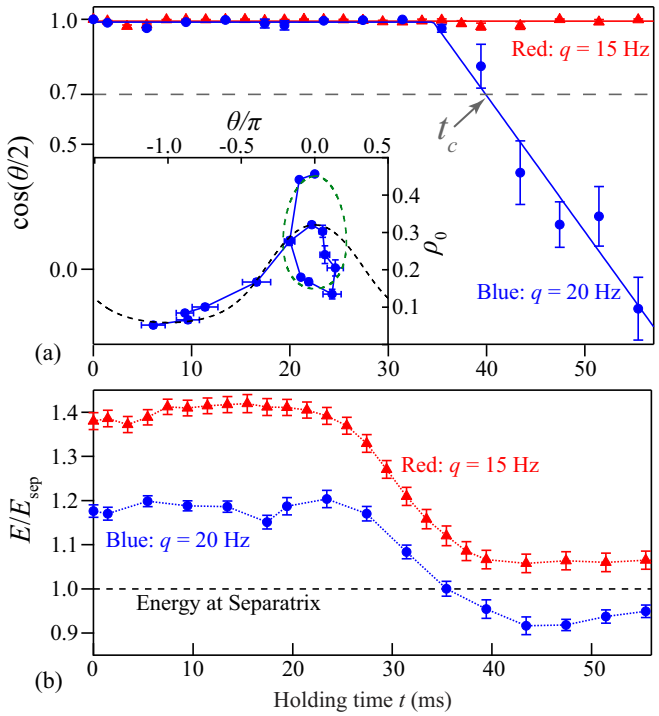

FIG. 5. (a) The appearance of a finite $t_c \approx 40$ ms in the $q = 20$ Hz dataset (circles) identifies a DPT driven by the moving-lattice-induced change in $c_2(t)$, while no DPT occurs in the $q = 15$ Hz set (triangles) as $\cos(\theta/2) > 0.7$ for all t. Solid lines are linear fits, while the dashed line marks $\cos(\theta/2) = 0.7$. Inset: Circles display the DPT and the phase diagram for the $q = 20$ Hz set shown in the main panel. The green (black) line displays the approximate equal energy contours for the interaction (Zeeman) regime occurring before (after) the drastic moving-lattice-induced change in c_2. (b) Blue circles (red triangles) show the extracted system energy E drops below (stays above) the separatrix energy (dashed line) at $q = 20$ Hz ($q = 15$ Hz) due to the moving-lattice-induced change in $c_2(t)$. Additional analysis demonstrates that the uncertainty in the reconstructed $c_2(t)$ does not significantly affect the inferred DPT in the moving-lattice system (see Appendix C).

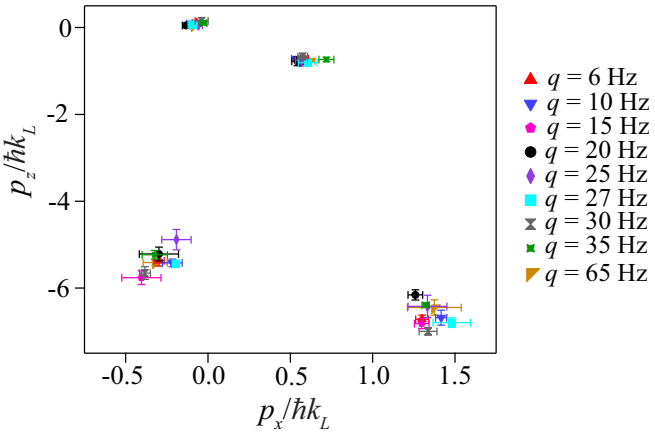

FIG. 6. The observed spatial dynamics in the moving-lattice system have no significant q dependence, as demonstrated here for a typical holding time of 9.43 ms. Here p_z (p_x) is the momentum in (orthogonal to) the direction of gravity.

VI. DISCUSSION AND OUTLOOK

Our results demonstrate time-resolved observations of DPTs in spinor gases using the system energy and phase-based observables extracted from spin population dynamics both in free space and in a complex moving-lattice system subject to unknown time-dependent interactions. The direct study of the temporal phase behavior as the system undergoes a DPT may have applications in understanding crossover phenomena and universality, with potential extensions to nonintegrable models. Additionally, our work introduces the cutoff time t_c as an observable that can quickly identify DPTs in our system. We also demonstrate a robust method to extract time-dependent interaction values from spin population dynamics in highly nonequilibrium systems. This method allows a better characterization of microscopic and effective Hamiltonian parameters, advancing the quantum simulation capabilities of spinor gases. We note that this extraction is reliable when ρ_0 is not close to 0.5 and the system is in the interaction regime; we extend it across regimes by exploiting the observed q independence of the moving-lattice-induced $c_2(t)$ (see Appendixes A–C). The success of predictions and models based on these extracted interactions in explaining the complicated moving-lattice spin dynamics suggests that similar methods can be extended to other complex systems with time-dependent parameters, such as Floquet systems under a periodically driven magnetic field, driven interactions, or resonant spin-flopping fields.

ACKNOWLEDGMENTS

We acknowledge support from the Noble Foundation and the National Science Foundation through Grants No. PHY-2513302 and No. DGE-2510202. T.B. acknowledges support from the Air Force Office of Scientific Research under Award No. FA9550-25-1-0340.

DATA AVAILABILITY

The data that support the findings of this article are not publicly available upon publication because it is not technically feasible and/or the cost of preparing, depositing, and hosting the data would be prohibitive within the terms of this research project. The data are available from the authors upon reasonable request.

APPENDIX A: DETAILS OF THE c_2 EXTRACTION

To construct a complete picture of the full quantum dynamics, we solve Eq. (2) for $\theta(t_1)$ by approximating time derivatives by discrete differences starting from an estimate of $c_2(t_0)$, the known initial state at t_0, and the measured spin populations. We then use the extracted $\theta(t_1)$ to solve Eq. (3) for $c_2(t_1)$. Iterating this process [i.e., using $c_2(t_i)$ to obtain $\theta(t_{i+1})$, and $\theta(t_{i+1})$ to obtain $c_2(t_{i+1})$] then yields the full time dependence of θ and c_2. The limitation that $\rho_0 \not\sim 0.5$ occurs because for $M = 0$ the c_2-dependent terms in Eq. (3) are proportional to $1 - 2\rho_0$, which vanishes as $\rho_0 \to 0.5$. Thus, when $\rho_0 \approx 0.5$, the phase evolution becomes insensitive to c_2, and the inversion for c_2 is ill-conditioned. We further limit

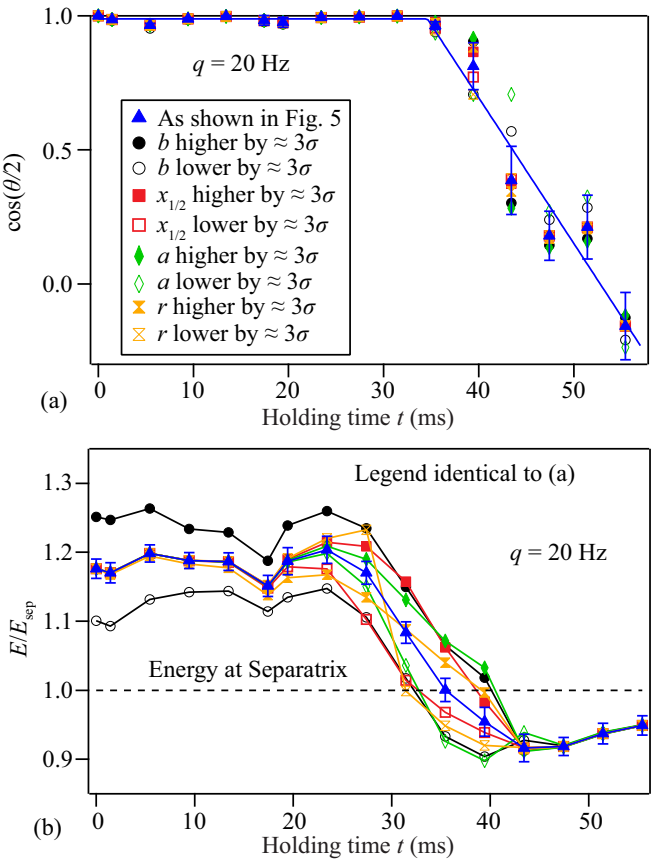

FIG. 7. (a) An analysis of the Fig. 5 data reveals that the uncertainty in the parameters of the reconstructed $c_2(t) = b + a/\{1 + \exp[(x_{1/2} - t)/r]\}$ does not significantly affect the inferred DPT for the moving-lattice data taken at $q = 20$ Hz. Here σ is an estimated 1 standard deviation for each fitting parameter. (b) A similar analysis for the energy of the spinor system also indicates that reasonable variations in the parameters of $c_2(t)$ do not affect the conclusion that a DPT occurs.

this extraction procedure to the interaction regime to avoid potentially nonunique solutions due to the wrapping of θ.

APPENDIX B: EXTENSION OF THE c_2 EXTRACTION ACROSS A BROAD RANGE OF q

To extend our analysis to regimes where the described method of extracting c_2 is not reliable, we approximate $c_2(t)$ with a sigmoidal fitting (i.e., $c_2(t) = b + a/\{1 + \exp[(x_{1/2} - t)/r]\}$) to the extracted c_2 data points taken at a single q value. Our observations and calculations indicate that the change in $c_2(t)$ induced by moving lattices has negligible dependence on the quadratic Zeeman shift q; i.e., similar $c_2(t)$ values are expected in the interaction and Zeeman regimes. This is exemplified in Fig. 6: the moving-lattice induced violent spatial dynamics (and associated atom losses) are found to have negligible dependence on q; the change in $c_2(t)$ is mainly determined by these spatial dynamics and thus is expected to be q independent. Similarities in the reconstructed $c_2(t)$ at various q values in the interaction regime also confirm this expectation. Together these results support the transfer of the reconstructed $c_2(t)$ to other q values where the c_2 extraction procedure cannot be easily applied.

APPENDIX C: ERROR ANALYSIS OF $c_2(t)$

Our analysis further shows that the uncertainty in the reconstructed $c_2(t)$ does not significantly affect the inferred DPT in the moving-lattice system, because the extracted θ is relatively insensitive to small variations in c_2 [see Fig. 7(a)]. While the energy plot is more sensitive to the form of c_2, any reasonable variation in c_2 does not affect the conclusion that a DPT occurs and at most changes the estimated timing of the DPT for the moving-lattice data taken at $q = 20$ Hz [see Fig. 7(b)].

[1] D. M. Stamper-Kurn and M. Ueda, Spinor Bose gases: Symmetries, magnetism, and quantum dynamics, Rev. Mod. Phys. **85**, 1191 (2013).

[2] Y. Kawaguchi and M. Ueda, Spinor Bose–Einstein condensates, Phys. Rep. **520**, 253 (2012).

[3] W. Zhang, D. L. Zhou, M.-S. Chang, M. S. Chapman, and L. You, Coherent spin mixing dynamics in a spin-1 atomic condensate, Phys. Rev. A **72**, 013602 (2005).

[4] M.-S. Chang, Q. Qin, W. Zhang, L. You, and M. S. Chapman, Coherent spinor dynamics in a spin-1 Bose condensate, Nat. Phys. **1**, 111 (2005).

[5] J. O. Austin-Harris, Z. N. Hardesty-Shaw, Q. Guan, C. Binegar, D. Blume, R. J. Lewis-Swan, and Y. Liu, Engineering dynamical phase diagrams with driven lattices in spinor gases, Phys. Rev. A **109**, 043309 (2024).

[6] Z. N. Hardesty-Shaw, Q. Guan, J. O. Austin, D. Blume, R. J. Lewis-Swan, and Y. Liu, Quench-induced nonequilibrium dynamics of spinor gases in a moving lattice, Phys. Rev. A **107**, 053311 (2023).

[7] Z. Chen, T. Tang, J. Austin, Z. Shaw, L. Zhao, and Y. Liu, Quantum quench and nonequilibrium dynamics in lattice-confined spinor condensates, Phys. Rev. Lett. **123**, 113002 (2019).

[8] J. O. Austin, Z. Chen, Z. N. Shaw, K. W. Mahmud, and Y. Liu, Quantum critical dynamics in a spinor Hubbard model quantum simulator, Commun. Phys. **4**, 61 (2021).

[9] J. O. Austin, Z. N. Shaw, Z. Chen, K. W. Mahmud, and Y. Liu, Manipulating atom-number distributions and detecting spatial distributions in lattice-confined spinor gases, Phys. Rev. A **104**, L041304 (2021).

[10] Q. Guan, D. Blume, and R. J. Lewis-Swan, Controlling the dynamical phase diagram of a spinor Bose-Einstein condensate using time-dependent potentials, Phys. Rev. A **112**, 023306 (2025).

[11] H.-X. Yang, T. Tian, Y.-B. Yang, L.-Y. Qiu, H.-Y. Liang, A.-J. Chu, C. B. Dağ, Y. Xu, Y. Liu, and L.-M. Duan, Observation of dynamical quantum phase transitions in a spinor condensate, Phys. Rev. A **100**, 013622 (2019).

[12] Q. Guan and R. J. Lewis-Swan, Identifying and harnessing dynamical phase transitions for quantum-enhanced sensing, Phys. Rev. Res. **3**, 033199 (2021).
[13] J. Marino, M. Eckstein, M. S. Foster, and A. M. Rey, Dynamical phase transitions in the collisionless pre-thermal states of isolated quantum systems: Theory and experiments, Rep. Prog. Phys. **85**, 116001 (2022).
[14] L. Zhou, J. Kong, Z. Lan, and W. Zhang, Dynamical quantum phase transitions in a spinor Bose-Einstein condensate and criticality enhanced quantum sensing, Phys. Rev. Res. **5**, 013087 (2023).
[15] P. Feldmann, C. Klempt, A. Smerzi, L. Santos, and M. Gessner, Interferometric order parameter for excited-state quantum phase transitions in Bose-Einstein condensates, Phys. Rev. Lett. **126**, 230602 (2021).
[16] W. Zhang, D. L. Zhou, M.-S. Chang, M. S. Chapman, and L. You, Dynamical instability and domain formation in a spin-1 Bose-Einstein condensate, Phys. Rev. Lett. **95**, 180403 (2005).
[17] A. T. Black, E. Gomez, L. D. Turner, S. Jung, and P. D. Lett, Spinor dynamics in an antiferromagnetic spin-1 condensate, Phys. Rev. Lett. **99**, 070403 (2007).
[18] Y. Liu, S. Jung, S. E. Maxwell, L. D. Turner, E. Tiesinga, and P. D. Lett, Quantum phase transitions and continuous observation of spinor dynamics in an antiferromagnetic condensate, Phys. Rev. Lett. **102**, 125301 (2009).
[19] Y. Liu, E. Gomez, S. E. Maxwell, L. D. Turner, E. Tiesinga, and P. D. Lett, Number fluctuations and energy dissipation in sodium spinor condensates, Phys. Rev. Lett. **102**, 225301 (2009).
[20] H. K. Pechkis, J. P. Wrubel, A. Schwettmann, P. F. Griffin, R. Barnett, E. Tiesinga, and P. D. Lett, Spinor dynamics in an antiferromagnetic spin-1 thermal Bose gas, Phys. Rev. Lett. **111**, 025301 (2013).
[21] L. Zhao, J. Jiang, T. Tang, M. Webb, and Y. Liu, Dynamics in spinor condensates tuned by a microwave dressing field, Phys. Rev. A **89**, 023608 (2014).
[22] L. Zhao, J. Jiang, T. Tang, M. Webb, and Y. Liu, Antiferromagnetic spinor condensates in a two-dimensional optical lattice, Phys. Rev. Lett. **114**, 225302 (2015).
[23] J. O. Austin-Harris, P. Sigdel, C. Binegar, S. E. Begg, T. Bilitewski, and Y. Liu, Control of dynamical phase transitions and nonergodic relaxation via spinor phases Phys. Rev. A **113**, 063302 (2026).
[24] J. Kronjäger, C. Becker, P. Navez, K. Bongs, and K. Sengstock, Magnetically tuned spin dynamics resonance, Phys. Rev. Lett. **97**, 110404 (2006).
[25] J. Jiang, L. Zhao, M. Webb, and Y. Liu, Mapping the phase diagram of spinor condensates via adiabatic quantum phase transitions, Phys. Rev. A **90**, 023610 (2014).
[26] J. O. Austin-Harris, I. Rana, S. E. Begg, C. Binegar, T. Bilitewski, and Y. Liu, Observation of ergodicity breaking and quantum many-body scars in spinor gases, Phys. Rev. Lett. **134**, 113401 (2025).
[27] C. Binegar, J. O. Austin-Harris, S. E. Begg, P. Sigdel, T. Bilitewski, and Y. Liu, Lattice-enabled detection of spin-dependent three-body interactions, Phys. Rev. A **113**, 043304 (2026).
[28] R. J. Lewis-Swan, S. R. Muleady, D. Barberena, J. J. Bollinger, and A. M. Rey, Characterizing the dynamical phase diagram of the Dicke model via classical and quantum probes, Phys. Rev. Res. **3**, L022020 (2021).
[29] C. B. Dağ, S.-T. Wang, and L.-M. Duan, Classification of quench-dynamical behaviors in spinor condensates, Phys. Rev. A **97**, 023603 (2018).
[30] R. Shimano and N. Tsuji, Higgs mode in superconductors, Annu. Rev. Condens. Matter Phys. **11**, 103 (2020).
[31] R. Matsunaga, Y. I. Hamada, K. Makise, Y. Uzawa, H. Terai, Z. Wang, and R. Shimano, Higgs amplitude mode in the BCS superconductors $Nb_{1-x}Ti_xN$ induced by terahertz pulse excitation, Phys. Rev. Lett. **111**, 057002 (2013).
[32] N. Fläschner, D. Vogel, M. Tarnowski, B. Rem, D.-S. Lühmann, M. Heyl, J. Budich, L. Mathey, K. Sengstock, and C. Weitenberg, Observation of dynamical vortices after quenches in a system with topology, Nat. Phys. **14**, 265 (2018).
[33] P. Jurcevic, H. Shen, P. Hauke, C. Maier, T. Brydges, C. Hempel, B. P. Lanyon, M. Heyl, R. Blatt, and C. F. Roos, Direct observation of dynamical quantum phase transitions in an interacting many-body system, Phys. Rev. Lett. **119**, 080501 (2017).
[34] J. Zhang, G. Pagano, P. W. Hess, A. Kyprianidis, P. Becker, H. Kaplan, A. V. Gorshkov, Z.-X. Gong, and C. Monroe, Observation of a many-body dynamical phase transition with a 53-qubit quantum simulator, Nature (London) **551**, 601 (2017).
[35] B. Evrard, A. Pizzi, S. I. Mistakidis, and C. B. Dag, Quantum scars and regular eigenstates in a chaotic spinor condensate, Phys. Rev. Lett. **132**, 020401 (2024).
[36] K. Fujimoto and S. Uchino, Floquet spinor Bose gases, Phys. Rev. Res. **1**, 033132 (2019).
[37] B. Evrard, A. Qu, K. Jiménez-García, J. Dalibard, and F. Gerbier, Relaxation and hysteresis near Shapiro resonances in a driven spinor condensate, Phys. Rev. A **100**, 023604 (2019).
[38] Z.-C. Li, Q.-H. Jiang, Z. Lan, W. Zhang, and L. Zhou, Nonlinear Floquet dynamics of spinor condensates in an optical cavity: Cavity-amplified parametric resonance, Phys. Rev. A **100**, 033617 (2019).
[39] C.-J. Liu, Y.-C. Meng, J.-L. Qin, and L. Zhou, Classical and quantum chaos in a spin-1 atomic Bose–Einstein condensate via Floquet driving, Results Phys. **43**, 106091 (2022).
[40] Z. N. Hardesty-Shaw, Q. Guan, J. O. Austin-Harris, D. Blume, R. J. Lewis-Swan, and Y. Liu, Nonlinear multistate tunneling dynamics in a spinor Bose-Einstein condensate, Phys. Rev. A **108**, 053307 (2023).